Rapid Standoff Spectroscopic Characterization of Plastic Waste Using Quartz Tuning Fork

Yaoli Zhao[1,*], Kyle Leatt[1], Patatri Chakraborty[1], Leqi Lin[2], K Prabakar[1,3], Thomas Thundat[1,4,*]

[1]Chemical and Biological Engineering Department, University at Buffalo, Buffalo, New York 14260, USA

[2]Mechanical and Aerospace Engineering Department, University at Buffalo, Buffalo, New York 14260, USA

[3]Materials Science Group, Indira Gandhi Centre for Atomic Research, HBNI, Kalpakkam, 603 102, India

[4]RENEW Institute, University at Buffalo, New York 14260, USA

*Corresponding authors: yaolizha@buffalo.edu (Yaoli Zhao), tgthunda@buffalo.edu (Thomas Thundat).

ABSTRACT

Standoff molecular identification of chemicals finds immense applications in homeland security, forensic investigation and plastic recycling industries. Although, standoff detection using mid-infrared radiation offers excellent molecular selectivity, sensitive detection of mid-IR radiation using inexpensive detectors is a challenge. In the present work, we show commercially available inexpensive Quartz Tuning Fork (QTF) can be effectively used for rapid standoff detection of solid samples using mid-IR radiation. In this method, a plastic sample placed 40 cm away was excited with tunable infrared (IR) radiation pulsed at the resonance frequency of the QTF. The IR radiation scattered off the plastic sample was used for exciting the QTF into resonance. Plotting the QTF resonant amplitude as a function of irradiating IR wavelength represents the unique IR spectrum of the plastic sample under study. The resolution of spectra recorded using QTF was found to be superior to those collected with ATR-FTIR and the technique based on QTF was 10^3 times faster than microcantilever-based photothermal deflection techniques. By combining simple machine learning algorithms with QTF standoff resonance IR spectra, various plastic samples can be effectively classified with 100% accuracy. Also, this technique was found to be capable of identifying black plastics without any further sample preparation requirements.

Keywords:

Quartz tuning fork, standoff detection, mid-infrared spectroscopy, plastic classification, machine learning

INTRODUCTION

Standoff chemical sensing techniques, where the operator and sensor element are at a distance from the sample, have been gaining interest in recent times for forensic investigations, environmental monitoring, national defense, and security applications[1-5]. Standoff detection of

waste plastic to identify their resin identification code has immediate relevance in the recycling industry[6-9]. In standoff chemical sensing, analyte never comes in direct contact with the sensor circumventing the need for sample collection. For example, sensitive and selective detection of trace chemicals such as surface adsorbed explosives have been carried out using standoff chemical sensing[10-12]. Molecular selectivity in standoff detection is obtained by resonant excitation of physiosorbed molecules by spectroscopic techniques. Standoff chemical sensing techniques are optical spectroscopic techniques such as laser absorption spectroscopy[13, 14], Laser induced fluorescence[15-17], coherent Raman spectroscopy[18, 19], Infrared absorption/reflection spectroscopy[20, 21] and Terahertz spectroscopy[22, 23], and so on. Although most of these spectroscopic techniques offer high selectivity towards the target species, they lack the required high sensitivity. For example, Conventional IR spectroscopy, following the Beer–Lambert principle, relies on photodetectors which require cooling to suppress the dark current originating from background noise. Often, intense stray light can saturate such conventional photodetectors making sensitive detection a challenge. Similarly, Raman spectroscopy provides distinct and well-resolved peaks of chemicals, however, it suffers from low photon fluxes, and the achievement of sufficient signal-to-noise (S/N) ratios at acceptable acquisition times often requires the use of high-throughput detection systems and relatively high laser power. [24].

Recently, standoff mid-infrared spectroscopy using microfabricated sensors such as microcantilevers has been gaining popularity due to their ultra-high sensitivity and molecular selectivity[25, 26]. In standoff spectroscopy using cantilevers, a sample placed at a distance is illuminated sequentially with mid-infrared radiation. The scattered light is then collected and detected with a microfabricated bi-material cantilever, which functions as an uncooled thermal sensor. In addition, mid-IR radiation (3-14μm), which is free of overtones and known as molecular fingerprint regime, is used as the illumination source. A bi-material cantilever has a very high thermal sensitivity, ~ 3-10 mK/nm, at room temperature[27] and has been successfully used for chemical sensing of adsorbed molecules using photothermal effect[28]. This technique known as photothermal cantilever deflection spectroscopy (PCDS) has been used for detecting ultra-trace levels of chemicals and biological molecules[29-31]. In this technique, the target molecules are first adsorbed on the bimetallic cantilever surface which are then excited using an IR source with tunable wavelength. The cantilever undergoes deflection because of the heat generated due to the non-radiative decay of resonantly excited molecules. The amplitude of cantilever deflection vs IR wavelength reveals the IR absorption peaks of the adsorbed molecules and therefore can be used for their selective detection. Although PCDS is a highly selective and sensitive technique, it requires the adsorption of target molecules on the cantilever. In standoff sensing, adsorbed molecules on a distant surface are resonantly excited using a tunable IR source and the scattered radiation is detected using a cantilever. As a result, standoff detection does not require the target molecules to adsorb on the cantilever and the cantilever acts only as a broadband IR detector. Standoff detection using cantilevers has been demonstrated before. For example, Van Neste et al.[12] demonstrated detection of trace explosives using bi-material cantilevers. Interestingly, the sensitivity of a microcantilever depends on its stiffness i.e., cantilevers with low spring constant offer higher deflection for a given change in temperature. However, cantilevers with lower stiffness have low Q-factor thereby compromising the signal-to-noise ratio[32]. Moreover, in these experiments, the cantilever deflection was monitored by using an optical beam deflection method.

The optical beam deflection is extremely sensitive, but its size and complexity make it unsuitable for field deployable applications. Attempts to use piezoresistive microcantilevers are often limited as the joule heating generated in piezo resistors affects the sensitivity of temperature measurement[33, 34].

Commercially available quartz tuning fork (QTF) has been routinely used as mass sensors. Recently they have been used as sensors for photoacoustic spectroscopy. QTF has many advantages such as a high Q-factor (~12000 in air), small size, low cost, low power consumption, high precision, long stability and fully digital frequency output signal[35]. QTFs are typically operated in symmetric vibration mode where prongs vibrate in opposite directions. Acoustically, in this mode, QTF acts as a quadrupole which results in excellent environmental noise immunity[36]. Sound waves from distant acoustic sources tend to move the QTF prongs in the same direction, thus resulting in no electrical response. Quartz-enhanced photoacoustic spectroscopy utilizes QTF along with IR radiation and is extensively studied for trace gas sensing applications with enhanced sensitivity and selectivity[37-40]. In this technique, QTF is operated at its resonance and acts as an acoustic sensor to detect the IR light-induced sound waves in its vicinity. QTF Vibration amplitude as a function of illuminating IR light shows the characteristic spectroscopic absorption signature of the gas under investigation. The thermoelastic effect of QTF is also explored for gas sensing applications and was first demonstrated by Yufei Ma[41]. In this technique, the light adsorption-induced photothermal energy is transformed into the mechanical motion of QTF. Efforts have been made to enhance detection sensitivity through modifications in the light path, the utilization of customized Quartz Tuning Forks (QTF), and innovative signal processing methods[42-44]. These advancements enable the detection of gas at parts per billion (ppb) levels.

In the present work, QTF was used for the fast standoff infrared spectroscopic characterization of solid plastic waste samples. Unlike conventional QTF-based photoacoustic spectroscopy, in the present method, QTF is utilized as a sensitive sensor with thermoelastic effect for the mid-IR light reflected off the plastic sample. In this technique, the plastic sample placed at a distance is excited with tunable IR radiation pulsed at the mechanical resonance frequency of the QTF. The vibration amplitude of the QTF was continuously monitored using the Lock-in method, as the IR wavelength is tuned. It was found that absorption of IR radiation at a specific wavelength by the sample decreases the intensity of the scattered IR light, which in turn reduces the vibration amplitude of QTF. QTF vibration amplitude vs IR wavelength therefore shows the IR spectra of a given plastic sample and can be used to sensitively classify the plastic samples. We have compared the spectra obtained with QTF and microcantilever-based method. The results show that the QTF-based detection has higher spectral resolution and is faster by 3 orders compared to the cantilever technique. Using simple machine learning algorithms, we are able to identify different plastic samples placed at a distance of 10-40 cm. We have also investigated the effect of modulation frequency, IR illumination location on QTF, scan speed and ambient temperature on the recorded spectra. Moreover, the present method was found to be useful for detecting black plastics, without any further sample preparation requirements.

EXPERIMENTAL SECTION

Commercially available QTF with resonance frequency at 32768 Hz were used in the present work. Ahead of experiments, the cap sealing of the QTF was removed and the exposed device was used as it is. QTF can be treated as two identical prongs (cantilevers) coupled by a low-loss quartz bridge. The resonance frequency of the QTF is determined by its geometry and material, and it can be estimated by the following equation[45, 46]

$$f_n = \frac{\pi T}{8\sqrt{12}L^2}\sqrt{\frac{E}{\rho}}m_n^2$$

Where E and ρ are Young's modulus and density of quartz, L, T are the prongs' length, and thickness, and m_n is the mode number, respectively. The L, w, t of the QTF used in this study are equal to 3500, 260, and 200 μm, respectively and for fundamental mode, $m_1 = 1.194$. When photons are incident on the QTF, it will generate heat and driving force is created caused by the thermoelastic property of QTF. If the incident photons are modulated, the photothermic force will set the QTF into mechanical motion and can be detected as an electrical signal due to the piezoelectric effect.

Standoff detection system using QTF was assembled on a standard optical table as illustrated in Figure 1(a). A tunable Quantum Cascade Laser (QCL) with wave numbers ranging from 775 cm^{-1} to 1900 cm^{-1} was employed as the mid-IR source (Block Engineering, LaserTune™). The QCL operates at an average power level of 100 mW, ensuring sufficient intensity for effective probing of the samples. The QCL was scanned from 775 cm^{-1} to 1900 cm^{-1} with a step of 10 cm^{-1} at a pulse width of 60 ns and a pulse repetition frequency of 1 MHz for the optimum power output. The IR beam was externally triggered by a function generator (Agilent 33600A Series). The plastic sample was placed on the sample stage and was shone by the IR beam emanating from the QCL. The scattered IR light from the plastic sample was collected using a gold coated concave mirror, placed 20 cm away from the sample. The collected light was then precisely focused onto the QTF placed at the focus point of the concave mirror (10 cm). It may be noticed that the concave mirror was conveniently placed above the plastic sample to enable it to collect most of the scattered IR light from the plastic sample. Also, QTF was mounted on a precision X-Y stage, so that the IR light from the concave mirror can be precisely focused on the desired position of the QTF prong. By using the concave mirror, it is certain that the light reaching the QTF after scattering from the plastic sample is sufficient to excite the QTF, as shown in Figure S4 in the supplementary information. The concave mirror used in the present work indeed efficiently collects and focuses the scattered light from the plastic sample enabling sensitive detection and characterization of plastics. For distance dependence experiments, the distance between the plastic sample and the concave mirror varied from 20 to 40 cm. The signal produced by the QTF was captured by a custom-made readout box and the signal was fed into a lock-in amplifier (Stanford Research Systems, model SR865 A). It may be noted that the QCL was pulsed at 1MHz frequency with duty cycle 5% (used to determine the output power) and modulated at 32.768 kHz which is the resonance frequency of QTF. The QTF response was found to be maximum when the IR modulation frequency matched the QTF resonance. The modulation frequency of 32.768 kHz was used as the reference signal in a lock-in amplifier which was found to improve signal-to-noise ratio

during data acquisition[47]. For comparison, plastic samples were also characterized using ATR-FTIR spectroscopy (VERTEX 70, Bruker).

It was observed that the QTF amplitude response also depends on the location of IR radiation on the QTF. The optimum radiation location for the visible laser was investigated before and found to be at the joint point of the two prongs of the QTF[48]. However, unlike visible light, for IR irradiation, the optimum location was found to be at the base of QTF and on the quartz material as shown in Figure 1(b) (see supplementary information). It may be attributed to the fact that when the wavelength of IR radiation is > 4.8 µm all the electromagnetic energy is known to be deposited in quartz[49]. Based on these experiments, all the spectroscopic measurements were performed by focusing the laser at the base of QTF and the modulating frequency was fixed at 32.76 KHz.

The spectra acquired in the present work were compared with the spectra obtained with the photothermal deflection spectroscopy (PCDS) method using a bi-material microcantilever. The details about PCDS can be found in other literature[50]. Briefly, the scattered photons from the plastic waste surface were collected and directed onto a bi-material cantilever. Cantilever deflection due to photon-induced heating was measured using an optical beam deflection method. By plotting the cantilever bending response as a function of scanning wavenumber, a photothermal spectrum of the sample was collected.

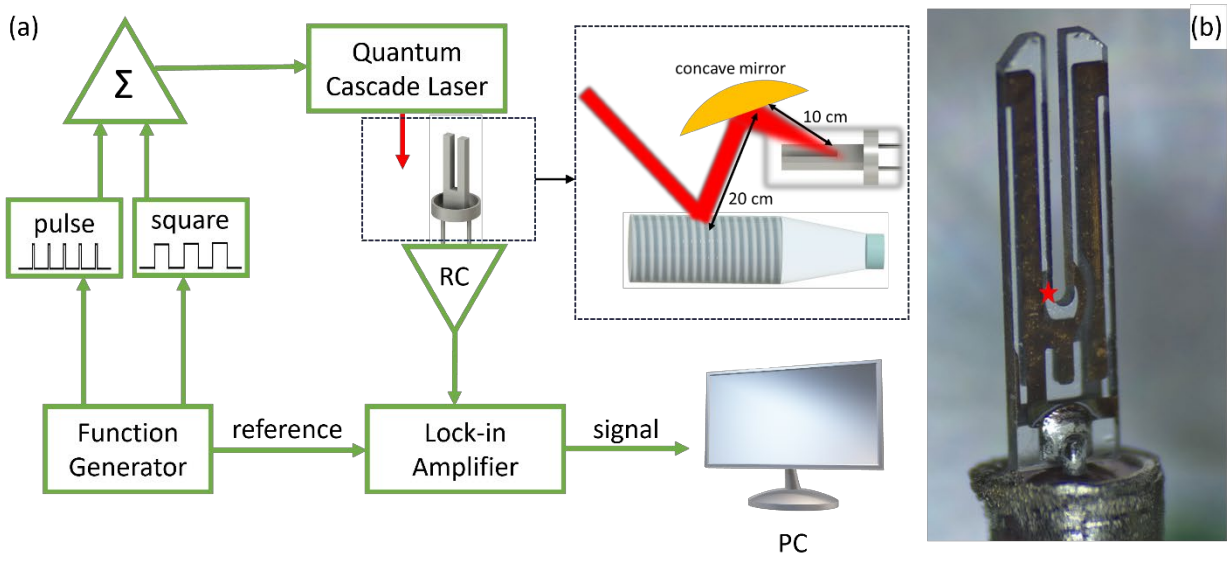

Figure 1. (a) Schematic of the experimental setup of thermoelastic IR spectroscopy using QTF. RC: readout circuit. The pulse rate is set 1MHz with 5% duty cycle and the modulation frequency of 32.76 kHz with a 50% duty cycle. The enlarged on the top right shows the standoff detection system. The incident photons hit the plastic waste surface and the scattered photons are collected and focused on the QTF. (b) Optical microscope image of a QTF used in this study. The laser excitation position is at the base of QTF and is shown by a star symbol.

We have used commonly available plastic samples, such as milk bottles, coffee cups, and plastic bags, representative of the plastics commonly encountered in material recycling facilities. The plastic samples include PET (water bottle), HDPE (milk bottle), PVS tubes, LDPE (plastic bags),

PP (coffee cup), and PS (plastic cutlery). For effective classification of plastics, the database collected by the QTF technique has been analyzed using a machine learning algorithm. More details can be found in the supplementary information.

RESULTS AND DISCUSSION

In our standoff detection experiments, the plastic samples were irradiated with IR radiation from a QCL in the wavelength range of 775 cm^{-1} to 1900 cm^{-1} and as explained earlier the scattered light was detected using a QTF placed in the optimum position. Initially, a background spectrum of the clean sample holder surface was recorded. Following this, the plastic waste sample under investigation was placed on the holder. It was illuminated with the QCL, and the vibrational amplitudes of the tuning fork were collected as a function of illumination wavelength. The ratio between the background and the plastic signal was calculated, producing a distinctive thermoelastic spectrum specific to the sample under investigation. Figure 2 shows the thermoelastic spectra recorded on six types of common plastic waste samples. The y-axis in Figure 2 represents the QTF vibration amplitude as a function of the mid-IR wavenumber (x-axis), which was used for illuminating the plastic waste samples. The extent of QTF vibration amplitude is directly proportional to the amount of IR radiation scattered by the plastics. The absorption peaks observed in the spectra correspond to the unique chemical characteristics of each plastic waste type. For example, in LDPE, the observed peak at 1377 cm^{-1} belongs to the symmetric bending mode of $-CH_3$ and the peak at 1473 cm^{-1} represents the bending mode of -C-H. Analysis of the standoff spectra of all the plastic samples studied in the present work is given in the supplementary material. These findings demonstrate that the standoff spectra obtained with a QTF effectively capture the vibrational bond information specific to each sample.

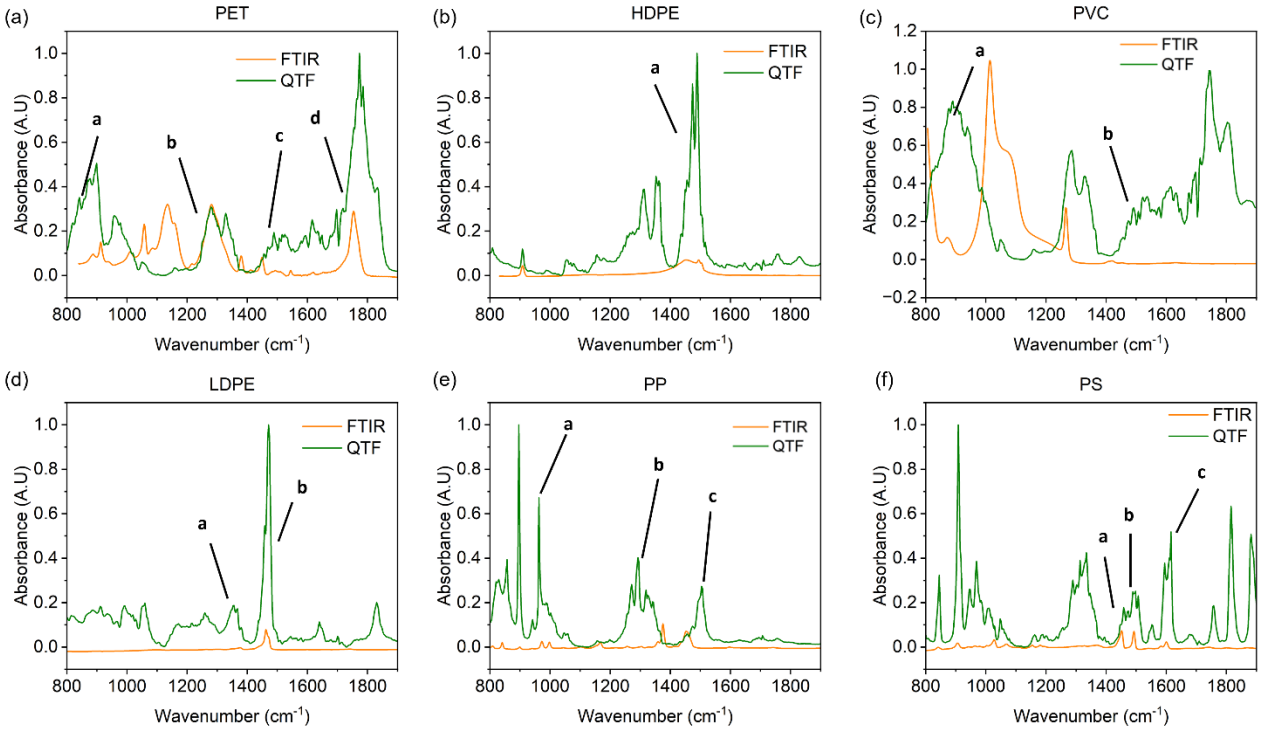

Figure 2. Thermoelastic spectra of different plastic waste samples recorded using QTF and their comparison with FTIR. (a) PET. (b) HDPE. (c) PVC. (d) LDPE. (e) PP. (f) PS.

Figure 3(a) compares the spectrum recorded in the present work using QTF with that obtained by ATR-FTIR. From this figure, it is evident that all the characteristic peaks seen in FTIR are clearly resolved in the spectra recorded using QTF but with different peak amplitudes. The differences in relative intensities of the two techniques can be attributed to the difference in the light source used, the photon detection method and the background correction methods employed. Photothermal spectra using QTF were recorded using QCL (polarized light), unlike FTIR which uses a thermal source (unpolarized light) with a different spectral resolution. Also, photons are detected using thermopile in FTIR, whereas it is the thermoelastic response of QTF in the present work. Relative intensities and presence/absence of peaks in QTF spectra when compared to FTIR seem to stem from these differences which make the photothermal spectra, of the analyte under study, obtained from QTF complementary to the FTIR spectrum.

Interestingly, additional peaks are also seen in the spectrum recorded using QTF in some samples. For example, the structure of polystyrene contains a CH_2 and a mono-substituted benzene ring pendant group. The peak at 1600 cm^{-1} is attributed to benzene ring mode. It is interesting to see the weak "benzene fingers" (series of weak overtone and combination bands) which fall from 1650 to 2000 cm^{-1} are clearly resolved in QTF spectra whereas they are not seen in the ATR-FTIR spectrum. Patterns of benzene fingers can be used to distinguish mono-, ortho-, meta-, and para-substituted benzene rings in polystyrene. Three peaks in this region probably indicate the mono-substituted benzene ring[51]. This result clearly demonstrates the superior peak-resolving nature of the experimental setup used in the present work using QTF.

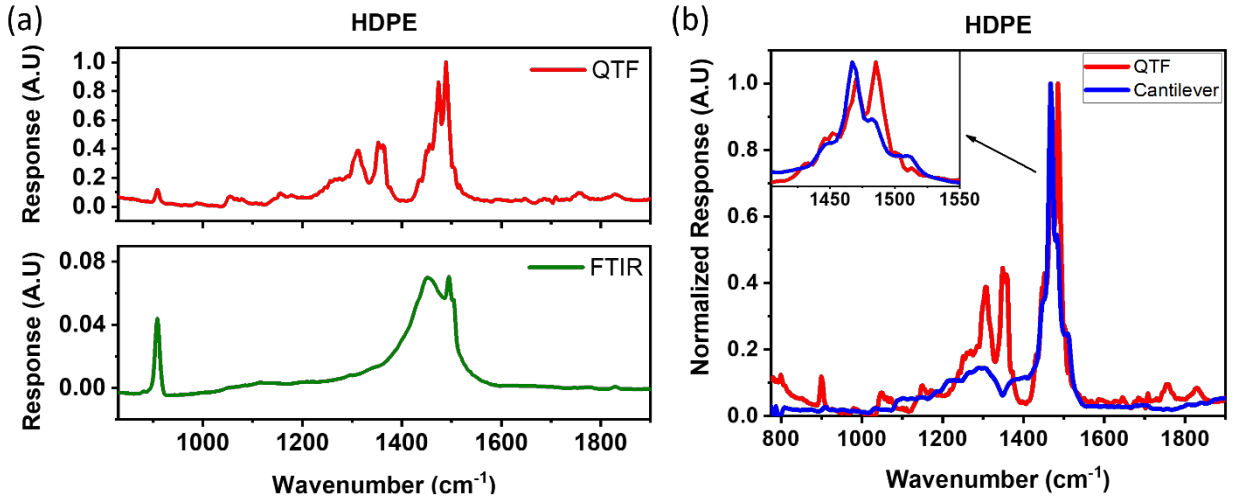

Figure 3. (a) IR spectrum of HDPE sample obtained by QTF and ATR-FTIR (b) Mid-IR spectrum of HDPE using QTF and photothermal cantilever deflection spectroscopy (PCDS).

Interestingly, the spectral resolution of QTF was found to be even better than the bi-material microcantilever-based PCDS. Figure 3(b) shows the typical standoff spectrum recorded on HDPE using both QTF and microcantilever. The peak at 1473 cm^{-1} corresponding to -C-H bending mode

in HDPE appears as two well-resolved peaks in thermoelastic spectroscopy when compared to the spectra recorded using microcantilevers (see inset). The lack of side chains in HDPE allows the methylene chains to get close enough to orient and crystallize. The methylene groups on two near-parallel CH_2 chains absorb photons of the appropriate energy at the same time and undergo vibrations simultaneously to form in-phase or out-of-phase vibration modes. This explains the reason for a pair of peaks in HDPE at 1472 cm^{-1} and 1464 cm^{-1}[52, 53]. These spectroscopic features are clearly seen using QTF and its superior nature can be attributed to the following reasons.

QTF used in the present work was operated at its resonance and had a very high Q-factor, unlike microcantilevers which were operated in static mode (i.e. off-resonance) in the PCDS technique. QTF has a higher spring constant and extremely high Q-factor which enables it to quickly resume to its equilibrium amplitude for a given temperature change[54]. Typical time response of QTF and microcantilever for an ON-OFF cycle of IR light at their corresponding modulating frequencies are shown in Figures 4(a) and (b), respectively. From the Lorenzen fitting curve, the response times were calculated and are shown in Table I. It is evident that the response time of QTF is 10^3 times faster than microcantilevers. QTF responds in microseconds, whereas microcantilevers take milliseconds.

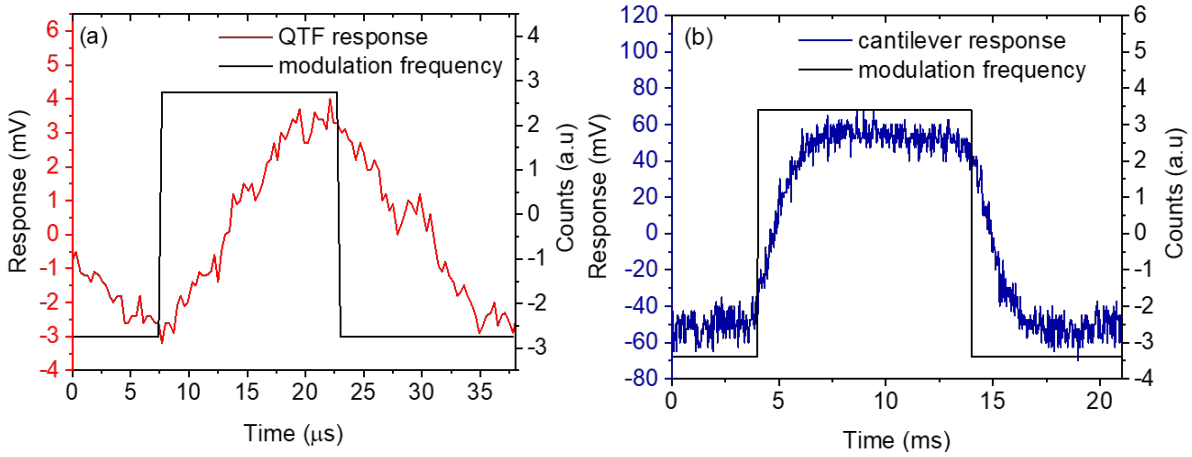

Figure 4. Time response of (a) QTF and (b) microcantilever. The solid line shows the ON-OFF cycle of IR light at a modulating frequency.

The noise-equivalent power (NEP) is the common metric that quantifies a photodetector's ultimate sensitivity as the power generated by a noise source[49]. It is defined as the signal power that gives a signal-to-noise ratio in a 1 Hertz-output bandwidth and is given by

$$NEP = \frac{S_N}{R_v}$$

where S_N is noise spectral density and R_v is the responsivity of the sensor. Responsivity of both QTF and microcantilever were estimated from response vs input IR laser power plot as shown in Figures 5 (a) and (b), respectively. It is evident that the responsivity of a QTF is higher by an order of magnitude than that of a microcantilever.

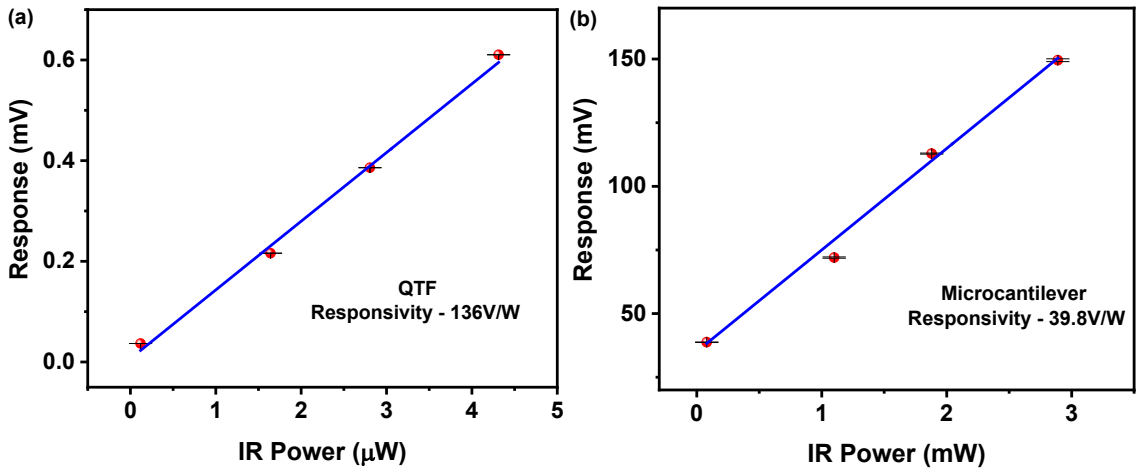

Figure 5. Incident IR power Vs response of (a) QTF and (b) microcantilever. From the linear fit of data, responsivity was estimated. Error bars are shown in black color.

Noise spectral density of QTF is given by[49],

$$S_n = \frac{\sqrt{\langle V_N^2 \rangle}}{\sqrt{\Delta f_D}} = R_f \sqrt{\frac{4K_B T}{R_{QTF}}}$$

where V_N is the voltage noise at the preamplifier output, f_D is the detection bandwidth, K_B is the Boltzmann constant and T is temperature. Also, R_{QTF} and R_f are thermal noise generated by QTF and preamplifier resistance, respectively. Typically, the R_{QTF} is in the range of 10 MΩ and the R_f used in the preamplifier is ~ 100 KΩ. Substituting these values in the above equation noise spectral density was estimated to be 33 μV/$\sqrt{Hz}$. Similarly, RMS noise amplitude (Z_{th}) of microcantilevers at off-resonance can be calculated using the formula[55],

$$Z_{th}/\sqrt{B} = \sqrt{\frac{4K_B T}{2\pi f_0 Q K_s}}$$

Where K_B is the Boltzmann constant, T is temperature, B is measurement bandwidth and Q, K_s, and f_0 are the quality factor, spring constant and resonance frequency of MC, respectively. By substituting these values for 500 μm and 100 μm MC, RMS noise amplitude was estimated to be 4.24x10^{-13} m/$\sqrt{Hz}$. Using these values NEP of QTF and microcantilever were estimated and are shown in Table 1. Interestingly, NEP of the microcantilever was superior to QTF as the former is operated off the resonance; but signal-to-noise ratio (SNR) was found to be much better in QTF. The SNR was calculated from the response signal to further evaluate the performance of the sensor by the following equation:

$$SNR = 10 \log \left(\frac{S}{N}\right)$$

Where S is the signal voltage and N is noise voltage. The estimated SNR is given in Table 1. The results show that the SNR of QTF is far better than that of microcantilever which is probably the reason for the better peak resolving power of QTF.

Table I. Various IR detection characteristics of QTF and microcantilever. *Voltage response was converted into microcantilever displacement in µm.

S.No.	Sensor	Modulating frequency	Noise spectral density	Responsivity	NEP	Response time	S/N
1.	QTF	32.78 kHz (resonance)	33µV/Hz$^{0.5}$	136V/W	0.24 µW/Hz$^{0.5}$	1.6µs	59 dB
2.	Micro-cantilever	50 Hz (off-resonance)	0.42 pm/Hz$^{0.5}$	39.8V/W (3.98 µm/W)*	28 nW/Hz$^{0.5}$	0.5ms	38 dB

For classifying the plastics samples using machine learning algorithms, the spectra data recorded using QTF was first fed into the principal components analysis (PCA). PCA is a statistical technique for reducing the dimensionality of a dataset, especially large ones containing a high number of dimensions/features per sample. It would enable visualization of multidimensional data while preserving the maximum amount of information. In our case, each sample was comprised of 385 features obtained by QTF while the PCA reduced the dimensionality to 3 as X-, Y-, and Z-coordinates of a dot shown in Figure 6 a. These coordinates describe three features having the maximum variations used for the classification. The distribution of our data illustrated that samples that shared the same category (label) were close to each other and roughly formed assembled clusters for they did share similar properties theoretically. Then ML algorithms were utilized to precisely classify the six types of plastics. Here we used the model of CNN aiming to extract representative features, based on facts which was already implied in our PCA experiments. From the confusion matrix, figure 6 b, the prediction accuracy on the entire dataset reached 100%.

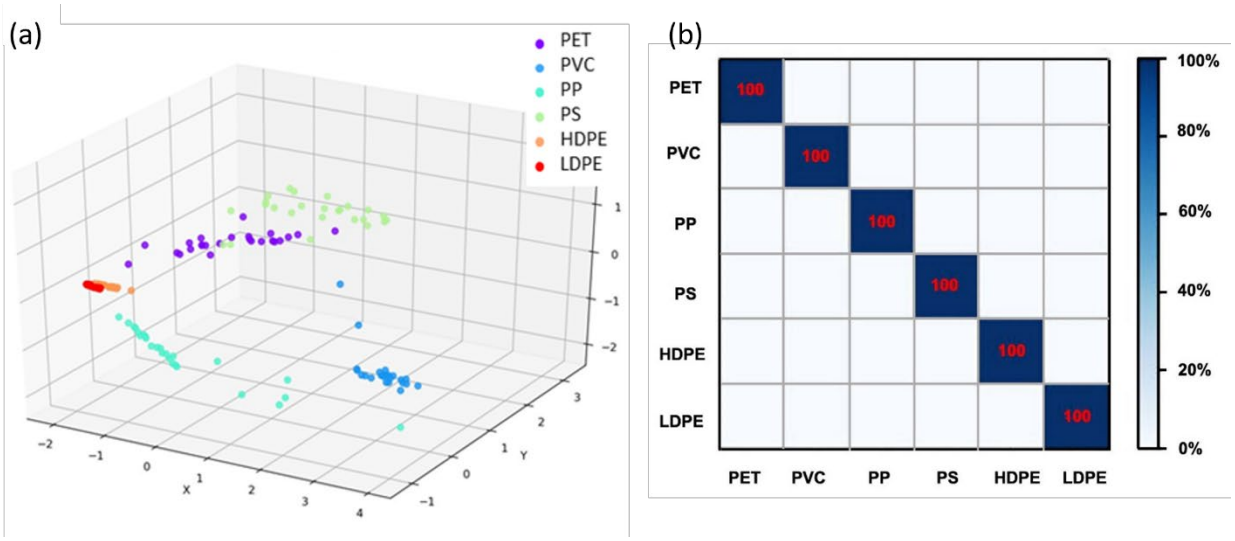

Figure 6. (a) Scatter plot of database obtained by the QTF technique for the classification of plastic samples (b) confusion matrix of the database containing six types of plastics obtained by QTF. The accuracy of the classification of pure plastics can reach 100%. The values for all other cells are zero.

To further assess the performance of the QTF-based technique, the effect of temperature, detection distance, laser power and scan speed were investigated. First, temperature dependence studies were conducted to evaluate the sensor's stability in relation to ambient temperature. Temperature fluctuations can induce mechanical strain in the QTF, which subsequently affects its resonant frequency[56]. To investigate the same, an experiment was performed to monitor the QTF response with increasing temperature (RT to 130 ºC) at a given IR excitation (1972 cm^{-1}). QTF was installed on the top of a programmable heating stage (MHP 30 PD, YKEY) at a fixed distance of 1 cm. Figure 7(a) shows the QTF response with increasing temperature. From this figure, it is evident that the fluctuation in the QTF signal resulting from changes in ambient temperature remains within 1.6%. This result indicates the remarkable stability of QTFs, highlighting their capability for dynamic operation under varying temperature conditions.

Second, the QTF response with distance from the plastic waste sample was investigated and is shown in Figure 7(b). It shows that with the detection distance increasing from 20 cm to 40 cm, the response only decreases by 7%. Therefore, by implementing suitable optics, this technique has the potential to extend the detection distance even longer, enhancing its suitability for long-range applications in MRFs.

To meet the requirements for rapid and efficient detection in MRFs, the QCL mode was transitioned from step mode to sweep mode. This transition allowed for faster processing, which could be completed within 10 seconds. As shown in Figure 7(c), the characteristic peaks of LDPE could still be reliably captured in sweep mode. Although the sweep time cannot be further reduced due to technical limitations of the QCL, this result underscores the potential for increased speed without sacrificing the technique's performance, thanks to the QTF's stability due to its high resonance frequency and Q-factor.

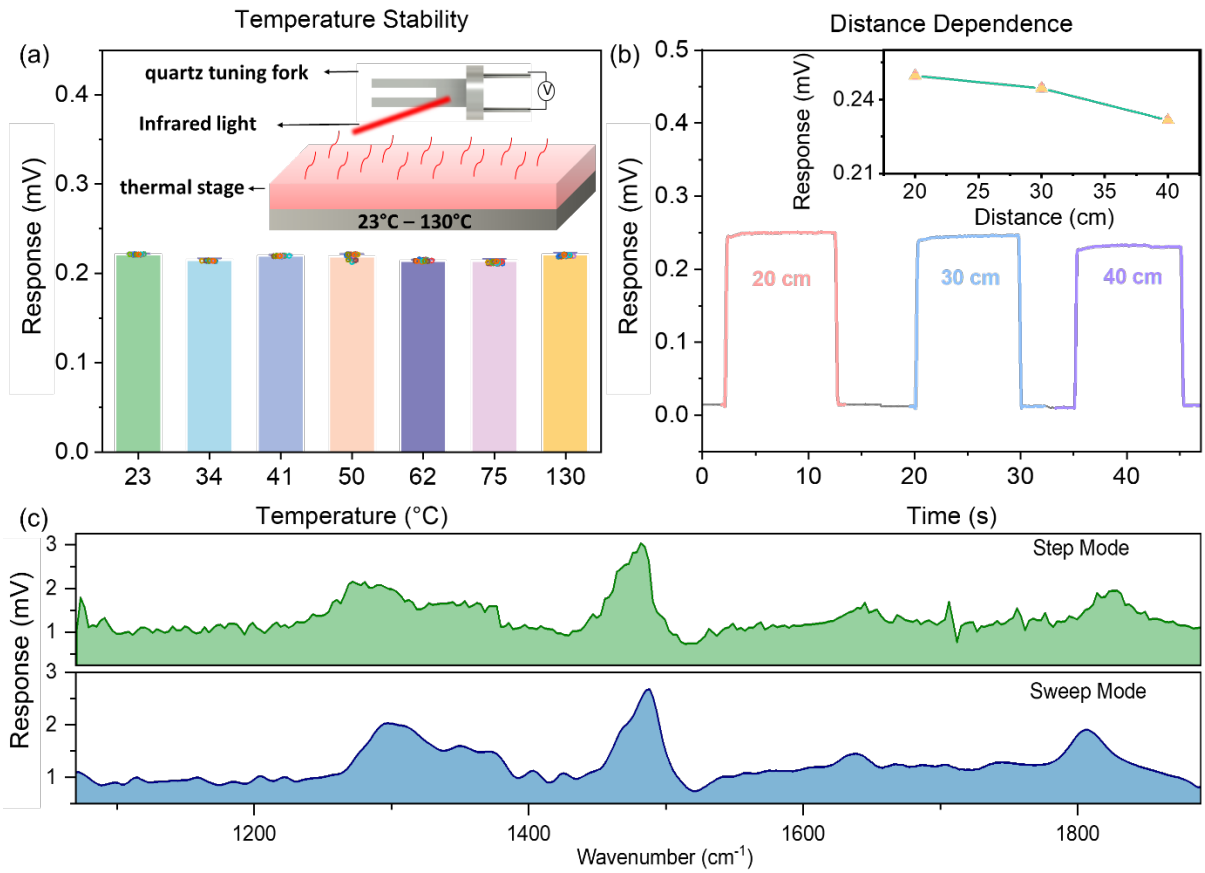

Figure 7. Performance of standoff thermoelastic spectroscopy detection system using QTF. (a) QTF response as a function of temperature at a fixed IR excitation. Insert figure shows the experimental setup schematic. (b) QTF response as a function of distance from the plastic sample. (c) QTF response under step and sweep operating mode of mid-IR.

Black plastics pose a substantial challenge while sorting using reflectance or transmittance spectroscopic methods like Near-Infrared (NIR) spectroscopy. The carbon particles that create the black color in these plastics absorb all NIR radiation, and as a result, no detectable signal can be obtained for material separation[57-59]. Figure 8 shows the thermoelastic spectrum of black-colored PVC, LDPE, and ABS samples using QTF standoff spectroscopy. It is evident from Figure 8 that, despite their identical visual appearance (see inset), the QTF-based technique using a mid-IR light source can successfully obtain the spectral signatures specific to each type of plastic material. Unlike NIR, mid-IR does not suffer from complete absorption by carbon particles. QTF being very sensitive, can pick up the spectroscopic features of various plastics even in the presence of carbon particles. The presence of additional peaks in these spectra might be due to the introduction of black dye in the black plastics and can be utilized to distinguish between different types of dyes. These results hold great promise for enhancing the accuracy of MPW characterization, a critical factor in the overall plastic recycling process. The performance of the technique can be further improved by utilizing customized QTFs[60].

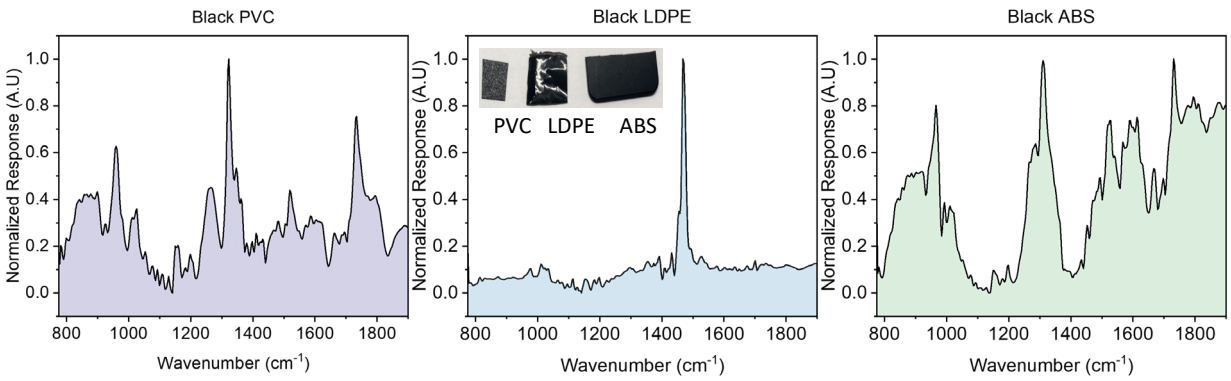

Figure 8. Thermoelastic spectra of black plastics: PVC, LDPE, and ABS. The insert figure shows the photograph of the tested samples.

CONCLUSIONS

We have demonstrated rapid standoff detection of waste plastics using an inexpensive quartz tuning fork and a tunable mid-IR radiation pulsed at the resonance frequency of the tuning fork. Scattered IR radiation from the plastic sample was used to excite the QTF and the resonant amplitude of the QTF as a function of irradiating wavelength showed the unique IR spectral features of the plastic sample. Using this technique, we were able to differentiate different classes of plastic samples, including black plastics, placed at a distance of 40 cm. The spectral peaks obtained using QTF showed higher spectral resolution as compared to ATR-FTIR. Moreover, it was found to be 10^3 times faster than static photothermal cantilever deflection spectroscopy. The spectra obtained with QTF when analyzed with a machine learning algorithm showed faster response times and extended detection distances. This technique has substantial promise for real-time, online molecular characterization in industries that demand both selectivity and sensitivity for high throughput operation.

ACKNOWLEDGEMENTS

This material is based upon work supported by the National Science Foundation (NSF) under Grant No. EFMA-2029375. The work is also supported by the New York State (NYS) Department of Environmental Conservation (DEC). One of the authors, KPR thanks USIEF- Fulbright for the exchange visit fellowship.

References

(1) Nelson, M. P.; Tazik, S. K.; Treado, P. J., Real-Time, Reconfigurable, Handheld Molecular Chemical Imaging Sensing for Standoff Detection of Threats, Chemical, Biological, Radiological, Nuclear, and Explosives (Cbrne) Sensing Xx, 11010(2019) 1101005, https://doi.org/10.1117/12.2519050.

(2) Razdan, A., & Veerabuthiran, S. . LIDAR: A Precision Long Range Standoff Sensor of Atmospheric Pollutants, Chemical, Biological and Explosive Agents. In *Advances in Laser Physics and Technology*, Razdan, A. Ed.; Foundation Books, 2014; pp 308-330.
(3) Sharma, R. C.; Kumar, D.; Bhardwaj, N.; Gupta, S.; Chandra, H.; Maini, A. K., Portable detection system for standoff sensing of explosives and hazardous materials, Optics Communications, 309(2013) 44-49, https://doi.org/10.1016/j.optcom.2013.06.025.
(4) Sharma, R. C.; Kumar, S.; Kumar, S.; Mann, M.; Mayank; Sharma, M., Photoacoustic remote sensing of suspicious objects for defence and forensic applications, Spectrochim Acta A, 224(2020), https://doi.org/10.1016/j.saa.2019.117445.
(5) Zygmunt, M., Laser systems for stand-off detection of contamination and pollution of atmosphere, Proc.SPIE, 6598(2007) 65980O, https://doi.org/10.1117/12.726559.
(6) Jiang, S. L.; Xu, Z.; Kamran, M.; Zinchik, S.; Paheding, S.; McDonald, A. G.; Bar-Ziv, E.; Zavala, V. M., Using ATR-FTIR spectra and convolutional neural networks for characterizing mixed plastic waste, Comput Chem Eng, 155(2021) 107547, https://doi.org/10.1016/j.compchemeng.2021.107547.
(7) Long, F.; Jiang, S. L.; Adekunle, A. G.; Zavala, V. M.; Bar-Ziv, E., Online Characterization of Mixed Plastic Waste Using Machine Learning and Mid-Infrared Spectroscopy, Acs Sustain Chem Eng, 10(2022) 16064-16069, https://doi.org/10.1021/acssuschemeng.2c06052.
(8) Taneepanichskul, N. H., H.C; Miodownik, M, Automatic identification and classification of compostable and biodegradable plastics using hyperspectral imaging, Frontiers in sustainability, 4(2023) 1125954, https://doi.org/10.3389/frsus.2023.1125954.
(9) Wu, X. Y.; Li, J.; Yao, L. P.; Xu, Z. M., Auto-sorting commonly recovered plastics from waste household appliances and electronics using near-infrared spectroscopy, J Clean Prod, 246(2020) 118732, https://doi.org/10.1016/j.jclepro.2019.118732.
(10) Liu, X. C.; Van Neste, C. W.; Gupta, M.; Tsui, Y. Y.; Kim, S.; Thundat, T., Standoff reflection-absorption spectra of surface adsorbed explosives measured with pulsed quantum cascade lasers, Sensor Actuat B-Chem, 191(2014) 450-456, https://doi.org/10.1016/j.snb.2013.10.026.
(11) Van Neste, C. W.; Senesac, L. R.; Thundat, T., Standoff Spectroscopy of Surface Adsorbed Chemicals, Anal Chem, 81(2009) 1952-1956, https://doi.org/10.1021/ac802364e.
(12) Van Neste, C. W.; Senesac, L. R.; Yi, D.; Thundat, T., Standoff detection of explosive residues using photothermal microcantilevers, Appl Phys Lett, 92(2008) 134102, https://doi.org/10.1063/1.2901145.
(13) Frish, M. B.; Wainner, R. T.; Laderer, M. C.; Green, B. D.; Allen, M. G., Standoff and Miniature Chemical Vapor Detectors Based on Tunable Diode Laser Absorption Spectroscopy, Ieee Sens J, 10(2010) 639-646, https://doi.org/10.1109/Jsen.2009.2038536.
(14) Li, J. Y.; Yang, X.; Li, L. H.; Wang, Z. B.; He, L. G.; Wu, Z. C.; Du, Z. H., Simultaneous standoff sensing for methane and hydrogen sulfide using wavelength-modulated laser absorption spectroscopy with non-cooperative target, Sensor Actuat B-Chem, 374(2023) 132825, https://doi.org/10.1016/j.snb.2022.132825.
(15) Farsund, O.; Rustad, G.; Skogan, G., Standoff detection of biological agents using laser induced fluorescence-a comparison of 294 nm and 355 nm excitation wavelengths, Biomed Opt Express, 3(2012) 2964-2975, https://doi.org/10.1364/Boe.3.002964.
(16) Hausmann, A.; Duschek, F.; Fischbach, T.; Pargmann, C.; Aleksejev, V.; Poryvkina, L.; Sobolev, I.; Babichenko, S.; Handke, J., Standoff detection: classification of biological aerosols using laser induced fluorescence (LIF) technique, Chemical, Biological, Radiological, Nuclear, and Explosives (Cbrne) Sensing Xv, 9073(2014) 90730Z, https://doi.org/10.1117/12.2049923.
(17) Sharma, R. C.; Kumar, D.; Kumar, S.; Joshi, D.; Srivastva, H. B., Standoff Detection of Biomolecules by Ultraviolet Laser-Induced Fluorescence LIDAR, Ieee Sens J, 15(2015) 3349-3352, https://doi.org/10.1109/Jsen.2015.2388547.

(18) Dogariu, A.; Pidwerbetsky, A., Coherent Anti-Stokes Raman Spectroscopy for detecting explosives in real-time, Chemical, Biological, Radiological, Nuclear, and Explosives (Cbrne) Sensing Xiii, 8358(2012) 83580R, https://doi.org/10.1117/12.919568.
(19) Vicentini, E.; Gambetta, A.; Galzerano, G.; Laporta, P.; Curtis, K.; McEwan, K.; Howle, C. R.; Coluccelli, N., Fiber laser system for standoff coherent Raman spectroscopy, Opt Lett, 45(2020) 5925-5928, https://doi.org/10.1364/Ol.404832.
(20) Kendziora, C. A.; Furstenberg, R.; Papantonakis, M.; Nguyen, V.; McGill, R. A., Broadband infrared imaging spectroscopy for standoff detection of trace explosives, Micro- and Nanotechnology Sensors, Systems, and Applications Viii, 9836(2016) 98362G, https://doi.org/10.1117/12.2224049.
(21) Kumar, M.; Islam, M. N.; Terry, F. L.; Freeman, M. J.; Chan, A.; Neelakandan, M.; Manzur, T., Stand-off detection of solid targets with diffuse reflection spectroscopy using a high-power mid-infrared supercontinuum source, Appl Optics, 51(2012) 2794-2807, https://doi.org/10.1364/Ao.51.002794.
(22) Liu, H. B.; Zhong, H.; Karpowicz, N.; Chen, Y. Q.; Zhang, X. C., Terahertz spectroscopy and imaging for defense and security applications, P Ieee, 95(2007) 1514-1527, https://doi.org/10.1109/Jproc.2007.898903.
(23) Federici J, G. D., Barat R, Zimdars D, THz Standoff Detection and Imaging of Explosives and Weapons, Proc. SPIE 5781, Optics and Photonics in Global Homeland Security, 5781(2005) 578110, https://doi.org/10.1117/12.590377.
(24) Lohumi, S.; Kim, M. S.; Qin, J. W.; Cho, B. K., Improving Sensitivity in Raman Imaging for Thin Layered and Powdered Food Analysis Utilizing a Reflection Mirror, Sensors-Basel, 19(2019) 2698, https://doi.org/10.3390/s19122698.
(25) Kim, S.; Lee, D.; Liu, X. C.; Van Neste, C.; Jeon, S.; Thundat, T., Molecular recognition using receptor-free nanomechanical infrared spectroscopy based on a quantum cascade laser, Sci Rep-Uk, 3(2013) 1111, https://doi.org/10.1038/srep01111.
(26) Zhao, Y. L.; Chakraborty, P.; Stavinski, N.; Velarde, L.; Maheshkar, V.; Dantu, K.; Phani, A.; Kim, S.; Thundat, T., Standoff and Point Detection of Thin Polymer Layers Using Microcantilever Photothermal Spectroscopy, J Electrochem Soc, 169(2022) 043401, https://doi.org/10.1149/1945-7111/ac5657.
(27) Perazzo, T.; Mao, M.; Kwon, O.; Majumdar, A.; Varesi, J. B.; Norton, P., Infrared vision using uncooled micro-optomechanical camera, Appl Phys Lett, 74(1999) 3567-3569, https://doi.org/10.1063/1.124163.
(28) Kim, S.; Lee, D.; Thundat, R.; Bagheri, M.; Jeon, S.; Thundat, T., Photothermal Cantilever Deflection Spectroscopy, Ecs Transactions, 50(2012) 459-464, https://doi.org/10.1149/05012.0459ecst.
(29) Bagheri, M.; Chae, I.; Lee, D.; Kim, S.; Thundat, T., Selective detection of physisorbed hydrocarbons using photothermal cantilever deflection spectroscopy, Sensor Actuat B-Chem, 191(2014) 765-769, https://doi.org/10.1016/j.snb.2013.10.078.
(30) Krause, A. R.; Van Neste, C.; Senesac, L.; Thundat, T.; Finot, E., Trace explosive detection using photothermal deflection spectroscopy, J Appl Phys, 103(2008) 094906, https://doi.org/10.1063/1.2908181.
(31) Rahimi, M.; Chae, I.; Hawk, J. E.; Mitra, S. K.; Thundat, T., Methane sensing at room temperature using photothermal cantilever deflection spectroscopy, Sensor Actuat B-Chem, 221(2015) 564-569, https://doi.org/10.1016/j.snb.2015.07.006.
(32) Beardslee, L. A.; Josse, F.; Heinrich, S. M.; Dufour, I.; Brand, O., Geometrical considerations for the design of liquid-phase biochemical sensors using a cantilever's fundamental in-plane mode, Sensor Actuat B-Chem, 164(2012) 7-14, https://doi.org/10.1016/j.snb.2012.01.035.
(33) Ansari, M. Z.; Cho, C., On self-heating in piezoresistive microcantilevers with short piezoresistor, J Phys D Appl Phys, 44(2011) 285402, https://doi.org/10.1088/0022-3727/44/28/285402.
(34) Xu, L.; Ren, J.; Jiang, Z. D.; Jia, Y.; Wei, X. Y., Effect of Joule heating on the performance of micromechanical piezoresistive oscillator, Sensor Actuat a-Phys, 333(2022) 113234, https://doi.org/10.1016/j.sna.2021.113234.

(35) Friedt, J. M.; Carry, E., Introduction to the quartz tuning fork, Am J Phys, 75(2007) 415-422, https://doi.org/10.1119/1.2711826.
(36) Russell, D. A., On the sound field radiated by a tuning fork, Am J Phys, 68(2000) 1139-1145, https://doi.org/10.1119/1.1286661.
(37) Lin, H. Y.; Huang, Z.; Kan, R. F.; Zheng, H. D.; Liu, Y. H.; Liu, B.; Dong, L. P.; Zhu, W. G.; Tang, J. Y.; Yu, J. H.; et al., Application of Micro Quartz Tuning Fork in Trace Gas Sensing by Use of Quartz-Enhanced Photoacoustic Spectroscopy, Sensors-Basel, 19(2019) 5240, https://doi.org/10.3390/s19235240.
(38) Sampaolo, A.; Menduni, G.; Patimisco, P.; Giglio, M.; Passaro, V. M. N.; Dong, L.; Wu, H. P.; Tittel, F. K.; Spagnolo, V., Quartz-enhanced photoacoustic spectroscopy for hydrocarbon trace gas detection and petroleum exploration, Fuel, 277(2020) 118118, https://doi.org/10.1016/j.fuel.2020.118118.
(39) Sharma, R. C.; Kumar, S.; Parmar, A.; Mann, M.; Prakash, S.; Thakur, S. N., Standoff pump-probe photothermal detection of hazardous chemicals, Sci Rep-Uk, 10(2020) 15053, https://doi.org/10.1038/s41598-020-71937-4.
(40) Wojtas, J.; Gluszek, A.; Hudzikowski, A.; Tittel, F. K., Mid-Infrared Trace Gas Sensor Technology Based on Intracavity Quartz-Enhanced Photoacoustic Spectroscopy, Sensors-Basel, 17(2017) 513, https://doi.org/10.3390/s17030513.
(41) Ma, Y. F.; He, Y.; Tong, Y.; Yu, X.; Tittel, F. K., Quartz-tuning-fork enhanced photothermal spectroscopy for ultra-high sensitive trace gas detection, Opt Express, 26(2018) 32103-32110, https://doi.org/10.1364/Oe.26.032103.
(42) Ma, Z. L. S. Q. Y., Fabry–Perot-based phase demodulation of heterodyne light-induced thermoelastic spectroscopy, Light: Advanced Manufacturing, 4(2023) 233-242, https://doi.org/10.37188/lam.2023.023.
(43) Liu, Y.; Qiao, S.; Fang, C.; He, Y.; Sun, H.; Liu, J.; Ma, Y., A highly sensitive LITES sensor based on a multi-pass cell with dense spot pattern and a novel quartz tuning fork with low frequency, Opto-Electron Adv, 7(2024) 230230, https://doi.org/10.29026/oea.2024.230230.
(44) Ma, Y.; Liang, T.; Qiao, S.; Liu, X.; Lang, Z., Highly Sensitive and Fast Hydrogen Detection Based on Light-Induced Thermoelastic Spectroscopy, Ultrafast Science, 3(2023) 0024, https://doi.org/10.34133/ultrafastscience.0024.
(45) Patimisco, P.; Sampaolo, A.; Mackowiak, V.; Rossmadl, H.; Cable, A.; Tittel, F. K.; Spagnolo, V., Loss Mechanisms Determining the Quality Factors in Quartz Tuning Forks Vibrating at the Fundamental and First Overtone Modes, Ieee T Ultrason Ferr, 65(2018) 1951-1957, https://doi.org/10.1109/Tuffc.2018.2853404.
(46) Sampaolo, A.; Patimisco, P.; Dong, L.; Geras, A.; Scamarcio, G.; Starecki, T.; Tittel, F. K.; Spagnolo, V., Quartz-enhanced photoacoustic spectroscopy exploiting tuning fork overtone modes, Appl Phys Lett, 107(2015) 231102, https://doi.org/10.1063/1.4937002.
(47) Zhang, Q. D.; Chang, J.; Cong, Z. H.; Wang, Z. L., Application of Quartz Tuning Fork in Photodetector Based on Photothermal Effect, Ieee Photonic Tech L, 31(2019) 1592-1595, https://doi.org/10.1109/Lpt.2019.2939046.
(48) He, Y.; Ma, Y. F.; Tong, Y.; Yu, X.; Tittel, F. K., Ultra-high sensitive light-induced thermoelastic spectroscopy sensor with a high -factor quartz tuning fork and a multipass cell, Opt Lett, 44(2019) 1904-1907, https://doi.org/10.1364/Ol.44.001904.
(49) Wei, T. T.; Zifarelli, A.; Dello Russo, S.; Wu, H. P.; Menduni, G.; Patimisco, P.; Sampaolo, A.; Spagnolo, V.; Dong, L., High and flat spectral responsivity of quartz tuning fork used as infrared photodetector in tunable diode laser spectroscopy, Appl Phys Rev, 8(2021) 041409, https://doi.org/10.1063/5.0062415.
(50) Zhao, Y.; Chakraborty, P.; Meng, Z.; Nair, A.; Goyal, A.; Thundat, T., Molecular Characterization of Plastic Waste Using Standoff Photothermal Spectroscopy, ECS Sensors Plus, 2(2023) 043401, https://doi.org/10.1149/2754-2726/acfb92.
(51) Smith, B., The Infrared Spectra of Polymers III: Hydrocarbon Polymers, Spectroscopy-Us, 36(2021) 22–25, https://doi.org/10.56530/spectroscopy.mh7872q7.

(52) Smith, B. C., Infrared Spectral Interpretation A Systematic Approach, Boca Raton: CRC Press; 1998.
(53) Smith, B. C., IR Spectral Interpretation Workshop Why Spectral Interpretation Needs To Be Taught, Spectroscopy-Us, 30(2015) 16-23,
(54) Marchetto, P.; Strickhart, A.; Mack, R.; Cheyne, H., Temperature Compensation of a Quartz Tuning-Fork Clock Crystal via Post-Processing, P Ieee Int Freq Cont, 1(2012) 1-4, https://doi.org/10.1109/FCS.2012.6243746.
(55) Barnes, J. R.; Stephenson, R. J.; Woodburn, C. N.; Oshea, S. J.; Welland, M. E.; Rayment, T.; Gimzewski, J. K.; Gerber, C., A Femtojoule Calorimeter Using Micromechanical Sensors, Rev Sci Instrum, 65(1994) 3793-3798, https://doi.org/10.1063/1.1144509.
(56) Ding, J. Y.; He, T. B.; Zhou, S.; Zhang, L.; Li, J. S., Quartz tuning fork-based photodetector for mid-infrared laser spectroscopy, Appl Phys B-Lasers O, 124(2018) 78, https://doi.org/10.1007/s00340-018-6950-9.
(57) Becker, W.; Sachsenheimer, K.; Klemenz, M., Detection of Black Plastics in the Middle Infrared Spectrum (MIR) Using Photon Up-Conversion Technique for Polymer Recycling Purposes, Polymers-Basel, 9(2017) 435, https://doi.org/10.3390/polym9090435.
(58) Faraca, G.; Astrup, T., Plastic waste from recycling centres: Characterisation and evaluation of plastic recyclability, Waste Manage, 95(2019) 388-398, https://doi.org/10.1016/j.wasman.2019.06.038.
(59) Ragaert, K.; Delva, L.; Van Geem, K., Mechanical and chemical recycling of solid plastic waste, Waste Manage, 69(2017) 24-58, https://doi.org/10.1016/j.wasman.2017.07.044.
(60) Fang, C.; Liang, T.; Qiao, S.; He, Y.; Shen, Z.; Ma, Y., Quartz-enhanced photoacoustic spectroscopy sensing using trapezoidal- and round-head quartz tuning forks, Opt Lett, 49(2024) 770-773, https://doi.org/10.1364/OL.513628.